ELSEVIER

Dyes and Pigments 49 (2001) 93–101

DYES and PIGMENTS

www.elsevier.com/locate/dyepig

Photodegradation of cyanine and merocyanine dyes

Songjie Yang [a], He Tian [a,*], Heming Xiao [b], Xinghong Shang [b], Xuedong Gong [b], Side Yao [c], Kongchang Chen [a]

[a] *Institute of Fine Chemicals, East China University of Science and Technology, Shanghai 200237, PR China*
[b] *Department of Chemiatry, Nanjing University of Science and Technology, Nanjing 210094, PR China*
[c] *Shanghai Institute of Nuclear Research, Academia Sinica, Shanghai 201800, PR China*

Received 7 September 2000; received in revised form 27 September 2000; accepted 18 February 2001

Abstract

The photodegradation kinetics for some cyanine and merocyanine dyes was studied by UV-visible spectroscopy and the results show that the fading process follows quasi-first-order or zero-order kinetics in acetonitrile. In other experiments, the principal photodegradation products of the dyes were identified with the aid of GC/MS, and it was found that those cyanine dyes holding a positive charge had higher photostability than the corresponding merocyanines. The relationship between photostability and chemical structure was established using PM3 and AM1 MO calculations. Experimental results in this regard suggest that the species associated with the photodegradation of cyanine dyes may be the semioxidized dye free radical cation, $Dye^{+\cdot}$. The transient absorption spectra of $Dye^{+\cdot}$ were determined by nanosecond pump and probe spectroscopy.

Keywords: Photodegradation; Cyanine dyes; MO calculations; GC/MS

1. Introduction

Cyanine dyes are among the most important and widely used synthetic dyes as spectral sensitisers in conventional silver halide photography [1]. Also, it has been reported that cyanine dyes offer advantages as absorbers for optical recording disks. For instance, they are inexpensive, easy to synthesize, and exhibit excellent optical properties, giving good recording sensitivity and a favorable signal to noise ratio [2,3]. In DNA sequencing, the introduction of fluorescent labels offers a practical and safe alternative to the traditional radioactive labels. To eliminate the high fluorescence background encountered in visible fluorescence analyses, a viable alternative has involved examining NIR absorbing cyanine dyes as labels in DNA sequencing [4,5]. In the current DNA sequencing technology, a typical indolocarbocyanine dye is often used as the fluorescent label [5]. As IR or NIR fluorescent dyes, indolocarbocyanine dyes have relative high photostability. However, the fundamental reasons why indolocarbocyanine dyes are better than other types of cyanine dyes in various applications have not been reported in detail.

In general, cyanine dyes, especially NIR absorbing cyanine dyes, readily undergo photodegradation. This is a key point because dye photostability plays an important role not only in the effectiveness of laser-induced fluorescence and dye laser technology but also in practically all applications involving

* Corresponding author. Fax: +86-21-64248311.
E-mail address: hetian@ecust.edu.cn (H. Tian).

0143-7208/01/$ - see front matter
PII: S0143-7208(01)00012-2

fluorescence spectroscopy, where either high sensitivity or a high signal rate is crucial [6,7]. Studies pertaining to the effects of substituents in the polymethine chain [8,9], end groups [10,11], and counter ions [12,13] on the photodegradation of cyanine dyes have been undertaken.

In the present study, flash photolysis, reaction pathways, and molecular orbital calculations were used to investigate the dependence of cyanine dye photodegradation on molecular charge. It was anticipated that the positive charge on the indolo heterocyclic moiety would play an important role in the photostability of cyanine dyes. Merocyanine dyes, whose indolo heterocyclic group holds no charge, were investigated in parallel studies. Structures of the four dyes employed are given in Fig. 1.

2. Experimental

Photolytic reactions were carried out in acetonitrile (HPLC grade, Fluka) at room temperature but interaction between solvent and dye molecules in acetonitrile were neglected. The photolysis experiments were carried out using a photochemical reaction apparatus (British Applied Photophys. Limited) equipped with a 200-watt Hg lamp. Absorption spectra were recorded on a Shimadzu UV-260 UV-visible spectrophotometer. Dye degradation was assessed by recording absorption spectra at various irradiation times. After 48 h, the photodegradation products were analysed by GC/MS using an HP 1800B GCD GC detector. The GC column was an HP-5 (30 m×0.25 mm×0.25 μm) and the temperature was raised from 40 to 300°C at a rate of 10°/min. The carrier gas used was high-purity nitrogen (99.99%). MS detection was performed under the vacuum of 52 mtorr, with a 167°C detector temperature and a voltage of 1507 V.

The transient absorption measurements were performed using a nanosecond time-resolved pump and probe apparatus with an excitation wavelength of 308 nm, pulse width of 20 ns, and output of 20 mJ/pulse. The excitation laser and detection light beam passed perpendicularly through the quartz sample cell. The transmitted light entered a monochromometer equipped with a R955 photomultiplier. The signals were recorded using a 300 MHz HP54510B digital storage oscilloscope and then processed with a SUN-486 personal computer [14]. Molecular geometries and electronic structures of the dyes were calculated using SCF-MO PM3 [15] and AM1 [16] methods.

3. Results and discussion

3.1. Photochemical reaction

All of the four dyes have strong absorptions in the 360–450 nm range, and the actual data are listed in Table 1. On the other hand, the

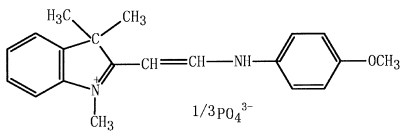

D-1

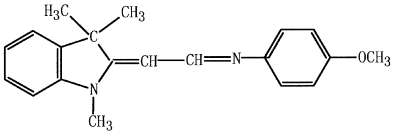

D-2

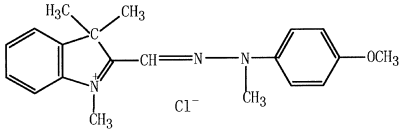

D-3

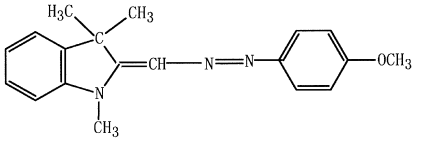

D-4

Fig. 1. Molecular structures of the dyes used in this study.

Table 1
Absorption maximum (λ_{max}) of dyes **D-1**–**D-4** in acetonitrile

Dyes	D-1	D-2	D-3	D-4
λ_{max} (nm)	416	372.4	443.6	430.2
(ϵ_{max} (10^4 cm^{-1} M^{-1}))	(2.02)	(3.34)	(2.39)	(4.02)

photodegradation products did not have absorptions in the visible region. Consequently, the dependence of dye concentration on irradiation time was determined by measuring visible absorbance values at various irradiation times. This information was used to determine the rate constants associated with photodegradation.

Based on an established mechanism for the oxidative photodegradation of a cyanine dye, the rate of photodegradation can be defined by Eq. (1):

$$-\mathrm{d[Dye]}/\mathrm{d}t = k_1[\mathrm{Dye}][\mathrm{O_2}] \quad (1)$$

Since the concentration of O_2 in the air-saturated solution is constant at $\sim 3\times10^{-4}$ M [7], Eq. (2) can be used to define the rate process:

$$\ln[\mathrm{Dye}]_0/[\mathrm{Dye}]_t = kt \quad (2)$$

A plot of $\ln[\mathrm{Dye}]_0/[\mathrm{Dye}]_t$ versus irradiation time (t) gives a straight line, the slope of which is the rate constant for oxidative photodegradation. In the present study, we observed a linear relationship between dye concentration and absorbance at λ_{max}. Therefore, the absorbance values were used directly as a function of changing irradiation times (t). The experimental results arising from dyes **D-1** and **D-2** are shown in Fig. 2. The data show a linear relationship between $\ln A_0/A_t$ and irradiation time, which means that the photodegradation of **D-1** and **D-2** follows quasi-first order kinetics.

The photodegradation of dyes **D-3** and **D-4** was followed at 443 and 430 nm, respectively. In both cases, there was a linear relationship between A_t and irradiation time (t), as shown in Fig. 3, which means that photodegradation followed zero-order kinetics. Since oxygen is a good electron acceptor and abundant in the reaction medium, the reaction of both dyes with dissolved oxygen in the excited state would normally characterize the primary process associated with photodegradation.

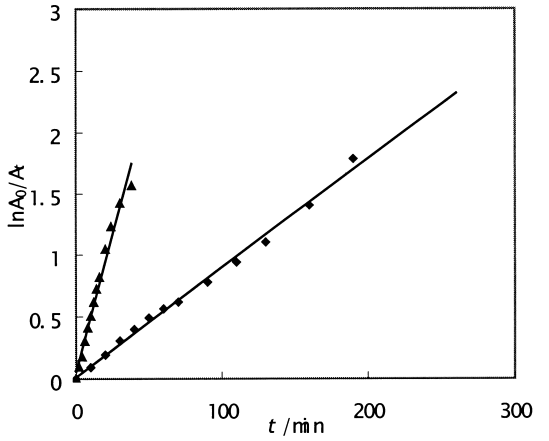

Fig. 2. The photodegradation of **D-1** (◆) at 416 nm and **D-2** (▲) at 372 nm.

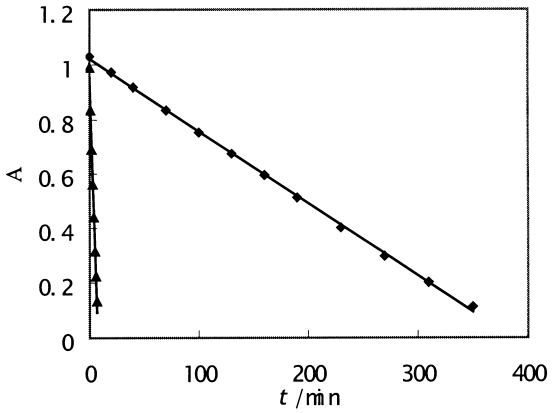

Fig. 3. The photodegradation of **D-3** (◆) at 443 nm and **D-4** (▲) at 430 nm.

Therefore, we believe that photodegradation proceeded according to Eqs. (3)–(5):

$$\mathrm{Dye} + h\nu \rightarrow \mathrm{Dye}^* \quad (3)$$

$$\mathrm{Dye}^* + \mathrm{O_2} \rightarrow \mathrm{Dye}^{\cdot+} + \mathrm{O_2}^{\cdot-} \quad (4)$$

$$\mathrm{O_2}^{\cdot-} + \mathrm{Dye} \rightarrow \text{degradation} \quad (5)$$

If dye excitation [Eq. (3)] is the rate-determining step, then photodegradation follows first order kinetics. This was the case for dyes **D-1** and **D-2**. For dyes **D-3** and **D-4**, Eqs. (3) and (5) proceeded quickly, and in this case the interaction of excited

dye with oxygen [Eq. (4)] became the rate determining step and photodegradation followed zero order kinetics.

The rate constants for the photodegradation of **D-1** and **D-3** were smaller than those for **D-2** and **D-4**, as shown in Table 2. This means that the positive charge present in **D-1** and **D-3** can greatly influence photostability. Specifically, the presence of a positive charge in the conjugated system stabilized these dyes to oxidation.

3.2. GC/MS of dye **D-4**

The photodegradation products of dye **D-4** were characterised in this aspect of our study. It was not possible to isolate the principal products, even in small quantities using conventional techniques. Instead, we used GC/MS to directly examine the product mixtures. Following the irradiation of dye **D-4** in acetonitrile at room temperature with a 200-W Hg lamp, eight major decomposition products were detected (Fig. 4). The major fragmentation ions observed in the mass spectrum of the product mixture are listed in Table 3. Based on these results a degradation pathway was developed (Fig. 5). We believe that dye degradation begins with the rupture of the N–C(Ar) bond of the N=N–Ar moiety. Then the C–N bond of the CH–N=N moiety and the C=C bond between the indole ring and CH–N=N moiety are attacked to produce the remaining products shown in Fig. 5. It should be mentioned that the products detected by GC/MS in these experiments arise from both the photodegradation and thermal decomposition of **D-4**. While the mechanisms associated with these two processes may be quite different, the bonds most easily broken were clearly revealed by the MS data. This information will be very useful in the design of photostable dyes.

3.3. Pump and probe spectroscopy experiments

In order to define how cyanine dyes undergo photodegradation, the triplet state of dyes should normally be considered as the species that reacts with oxygen [7]. In our studies, nanosecond pump and probe spectroscopy was used to record the transient absorption of the cyanine dyes following excitation at 308 nm. We used dyes **D-3** and **D-4** in this aspect of the study. The transient absorption spectra recorded on a solution of **D-3** at various times after laser excitation are shown in Fig. 6.

Table 2
Rate constants (k) for the photodegradation of dyes used in this study

Dye	**D-1**	**D-2**	**D-3**	**D-4**
k	8.9×10^{-3} min^{-1}	4.45×10^{-2} min^{-1}	2.7×10^{-3} mol·l^{-1} min^{-1}	1.2×10^{-1} mol·l^{-1} min^{-1}

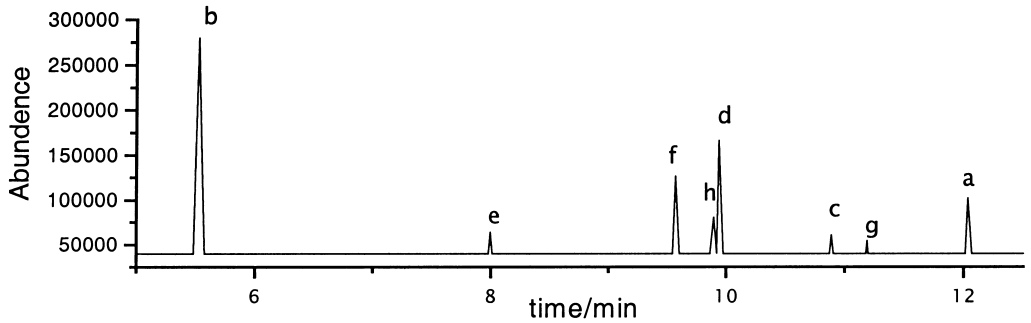

Fig. 4. Total ion chromatogram from GC/MS analysis of the decomposition products of **D-4**.

Table 3
The major ions (m/z) produced from degradation products **a**–**h**

a	b	c	d	e	f	g	h
203(M^+)	108(M^+)	219(M^+)	189(M^+)	161(M^+)	175(M^+)	207(M^+)	161(M^+)
175	93	174	161	146	160	176	161
160	78	161	146	128	145	147	146
132	51	146	128	117	132	132	128
117	39	130	117	91	117	118	117
103		117	105	77	103	103	91
91		103	91	65	91	95	77
77		91	77	58	77	77	65
65		77	63	51	65	63	58
51		65	51	39	51	51	51
39		44	39		39		39

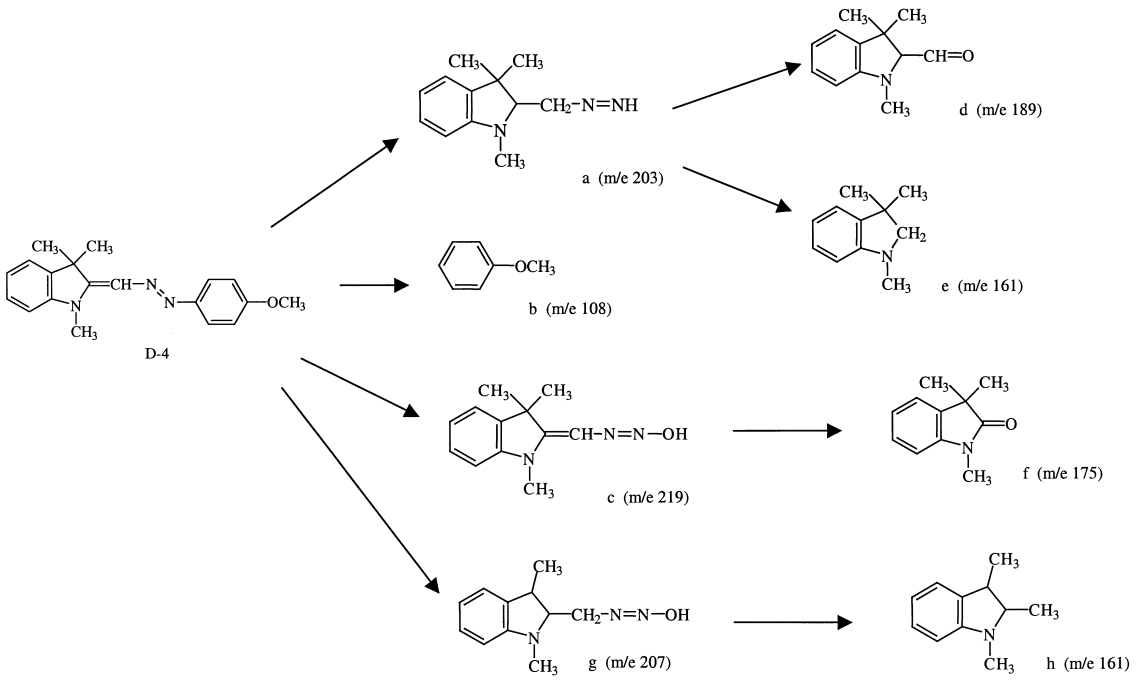

Fig. 5. Proposed pathway for the photodegradation of dye **D-4**.

Each spectrum shows a transient absorption centered at 390 nm and recovery of the absorption centered at 460 nm, over a 30-μs period.

The curves for the 390 nm transient species and the recovery of the ground state absorption at 460 nm are shown in Fig. 7. The two curves follow quasi-first-order kinetics, the half-lives of which are shown in Table 4. Laser excitation of dye **D-3** in O_2-saturated acetonitrile was performed for comparison. The resultant transient absorption and decay curves were very similar to those in Figs. 6 and 7, which indicates that O_2 did not influence the pump and probe spectroscopy of **D-3** following excitation at 308 nm. As seen in Table 4, the decay of the transient absorption at 390 nm did not vary significantly in the presence and absence of O_2. Also, the addition of ferrocene (a triplet state quencher, 2×10^{-5} M) did not give an obvious

change, indicating that the formation of triplet states or free radicals do not characterise dye degradation. It is more likely that the transient absorption at 390 results from the semioxidized dye free radical cation ($Dye^{+\cdot}$) [17] and that this species is the key intermediate in the photodegradation process. These results are also consistent with a photofading mechanism that is not dependent upon oxygen. The lifetime of the semioxidized dye free radical cation for **D-3** was about 14–15 μs, but the corresponding triplet state and free radical species were not observed.

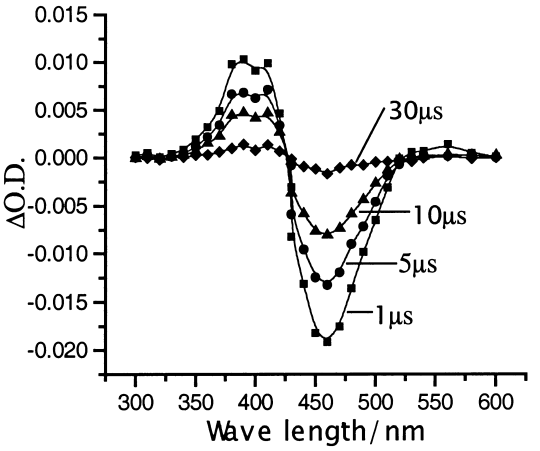

Fig. 6. Transient absorption spectra of a de-aerated **D-3** solution at various times after irradiation.

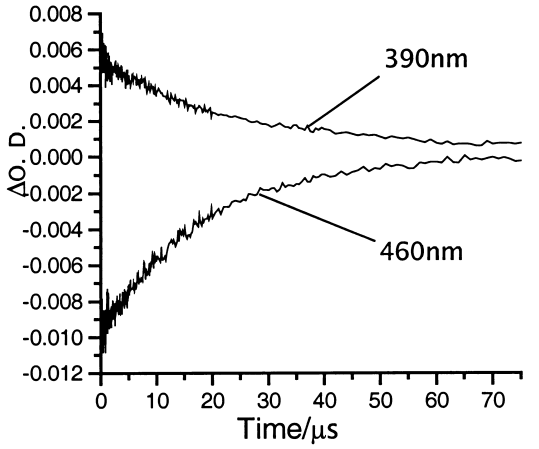

Fig. 7. Transient behavior of irradiated **D-3** at 390 and 460 nm.

Table 4
The decay half-life (τ) of **D-3** solutions at the transient absorption wavelengths

	In N_2-rich solution	In O_2-rich solution	With ferrocene
τ (390 nm)	14.7 μs	15.6 μs	14.1 μs
τ (460 nm)	13.2 μs	13.5 μs	12.2 μs

Laser excitation (308 nm) of dye **D-4** in acetonitrile led to two absorption bands and bleaching of ground state absorptions centered at 360, 500 and 420 nm, respectively (Fig. 8). The decay curves for the 360 and 500 nm transient absorptions and the recovery of the ground state absorption at 420 nm are depicted in Fig. 9. All three decays follow first-order kinetics, the half-lives of which are shown in Table 5. When laser excitation of **D-4** in O_2-saturated acetonitrile was performed, the resultant transient absorption spectrum was very similar to that obtained in deaerated solution. These results indicated that the transient absorption at 360 and 500 nm were not due to the triplet state or free radicals of **D-4**. It is also likely that both transient absorptions are due to the semioxidized dye free radical cation ($\mathbf{D\text{-}4}^{+\cdot}$). The lifetime of $\mathbf{D\text{-}4}^{+\cdot}$ (4–5 μs) was much short than that of $\mathbf{D\text{-}3}^{+\cdot}$, and the photostability of **D-4** was lower than that of **D-3**, which may be associated with the short lifetime of $\mathbf{D\text{-}4}^{+}$. Our experimental results were similar to those from a recent study involving the irradiation of related thiacarbocyanine dyes in methylene chloride,

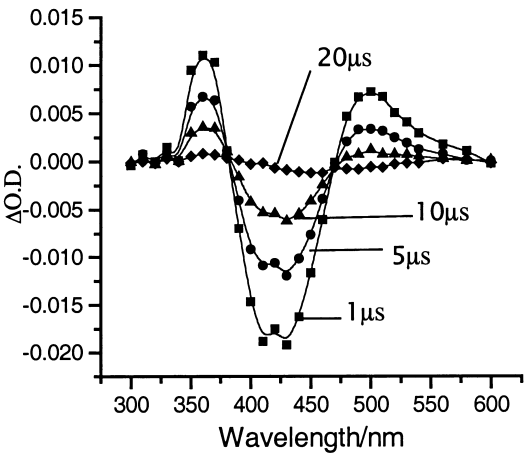

Fig. 8. Transient absorption spectra of a de-aerated **D-4** solution at various times after irradiation.

in which long-lived reduction in the intensity of the ground state absorptions was observed [18]. De Schryver has attributed this kind of behavior to conformation changes in the ground state of the cyanine dye [19]. It was also suggested that thiacarbocyanine dyes have at least two spectroscopic minima at the excited surface.

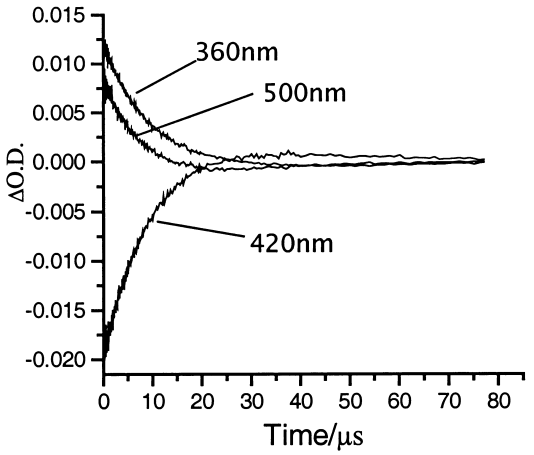

Fig. 9. Transient behavior of irradiated **D-4** at 360, 420 and 500 nm.

Table 5
The decay half-lives (τ) for **D-4**

	In N_2-rich solution	In O_2-rich solution
τ (360 nm)	5.92 μs	5.78 μs
τ (420 nm)	5.04 μs	5.82 μs
τ (500 nm)	4.22 μs	4.04 μs

3.4. MO calculations

With the aid of the SCF-MO methods PM3 and AM1, fully optimized molecular geometries for the cyanine dyes examined in this study were calculated. The PM3 optimized geometries for all four dyes are shown in Fig. 10. Selected bond distances, bond angles, dihedral angles, and partial charges associated with **D-1** and **D-2** are given in Tables 6 and Table 7. The frontier MO energy levels (E_{HO} and E_{LU}) and the constituent of HOMO and LUMO (i.e. the coefficients of atomic orbital) are shown in Tables 8 and 9, respectively.

It is evident from the data in Table 6 that there were significant differences in the molecular structures of cationic dye **D-1** and neutral dye **D-2**. For dye **D-1**, N(15), C(8), C(9), C(10) and N(11) form an extended conjugated system and angle C(5)–N(15)–C(8) (110.2°) departs far from 120°, as would be expected. N(15) has approximately sp^2 hybridization. As for dye **D-2**, the C(9)–C(10) bond length (1.459 Å) is larger than that of C(8)–C(9) (1.344 Å), and the N(11)–C(12) bond length (1.433 Å) is larger than that of N(11)–C(10) (1.294 Å). This indicates that **D-2** would have inferior conjugation.

The results in Table 7 indicate that the positive charge on dye **D-1** resides primarily on the N(11) and N(15) atoms and that C(12) and C(5) have

Table 6
Bond lengths (Å) and bond angles (°) for PM3 optimized **D-1** and **D-2** structures

Parameter	**D-1**	**D-2**	Parameter	**D-1**	**D-2**
4–5	1.387	1.389	9–10	1.394	1.459
5–6	1.405	1.406	10–11	1.347	1.294
5–15	1.451	1.449	11–12	1.443	1.433
7–8	1.542	1.532	12–13	1.405	1.402
8–9	1.394	1.344	12–14	1.399	1.397
8–15	1.372	1.454	15–16	1.464	1.477
8–9–10	126.4	125.1	5–15–8	110.2	106.8
9–10–11	121.8	119.0	5–15–16	121.6	116.2
10–11–12	123.4	121.7	8–15–16	128.1	119.5
1–6–5–15	178.6	177.1	8–9–10–11	177.6	154.2
5–6–7–8	0.838	0.895	9–10–11–12	175.6	180.0
7–8–15–5	0.316	2.883	Ph–Ph	26.76	22.47

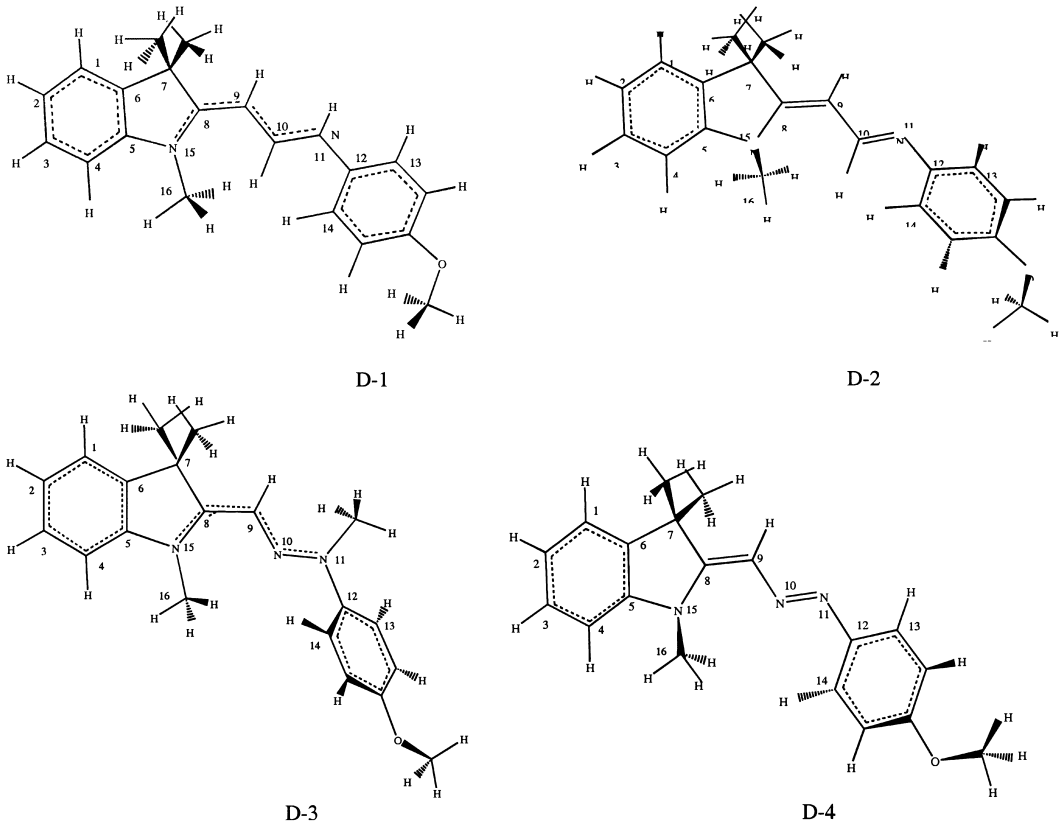

Fig. 10. PM3 optimized geometries of **D-1** – **D-4**.

Table 7
Selected partial charges computed using the PM3 method

Atom	**D-1**	**D-2**	Atom	**D-1**	**D-2**
C(5)	−0.166	−0.076	C(10)	−0.053	−0.035
C(6)	−0.108	−0.122	N(11)	0.392	−0.049
C(7)	0.029	0.048	C(12)	−0.245	−0.082
C(8)	0.047	−0.087	C(13)	−0.044	−0.061
C(9)	−0.361	−0.173	N(15)	0.313	0.110

more electron rich character. Therefore, it is not surprising that the positive and negative charges are delocalised across the N(15), C(8), C(9), C(10), N(11) and C(12) conjugation system.

We used frontier MO calculations to examine the interactions between the HOMO of superoxide radical anion ($O_2^{-\cdot}$) and the LUMO of **D-1**/**D-2** and **D-3**/**D-4** combinations.

Using PM3, we found that $E_{HO} = -0.8\ 17$ eV for O_2^-, and $E_{LU} = -4.82$ eV and -0.227 eV for **D-1** and **D-2**, respectively, and that $E_{LU} = -4.931$ and -0.612 eV for **D-3** and **D-4**. The symmetry of 2p-AO in the HOMO of O(1)–O(2) matched that of 2p-AO in the LUMO (C(10)–N(11) or N(10)–N(11)) of **D-1** (or **D-3**), and the gap (4.065 or 4.114 eV) between their energy levels was larger. However, the gap between the E_{LU} of **D-2** (or **D-4**) and E_{HO} of $O_2^{-\cdot}$ was 0.590 (or 0.205) eV and smaller than that for **D-1** (or **D-3**). It was also determined that the symmetry of the LUMO for C(8)–C(9) and C(10)–N(11) or N(10)–N(11) matched that of the HOMO of $O_2^{-\cdot}$ and the number of active positions on **D-2** (or **D-4**) was greater than the number on **D-1** (or **D-3**). This suggests that electron transfer from the HOMO of $O_2^{-\cdot}$ to the LUMO of **D-2** (or **D-4**) is more facile than that to the LUMO of **D-1** (or **D-3**). This could explain why the photostability of **D-2** (or **D-4**) is lower than that of **D-1** (or **D-3**). Similarly results were

obtained from AM1 calculations and were consistent with experimental data.

4. Conclusion

It has been found that the photostability of cyanine and merocyanine dyes that hold a positive charge in their system was higher than the corresponding neutral forms. These results were determined experimentally and from MO calculations utilising PM3 and AM1 methods. The photodegradation of these dyes took place after excitation at 308 nm and it was shown by nanosecond pump and probe spectroscopy that the triplet states or free radicals of the dyes were not involved in this process. Instead, it is believed that photodegradation occurs via formation of the semioxidized dye free radical cation.

Acknowledgements

This work was supported by NSFC/China (project No. 29836150).

References

[1] Sturmer DM, Heseltine DW. In: James TH, editor. The theory of the photographic process. 4th ed. New York: Macmillan Publishing; 1977 [Chapter 8].
[2] Nakazumi H. Journal of the Society of Dyers and Colorists 1988;104:121.
[3] Kuder JE. Journal of Imaging Technology 1986;12(3):40.
[4] Shealay DB, Lohrmann R. Applied Spectroscopy 1995;49:1815.
[5] Sauer M, Wolfrum J. In: Rettig W, Strehmel B, Schrader S, Seifert H, editors. Applied fluorescence in chemistry, biology and medicine. Berlin: Springer; 1999 [Chapter 2].
[6] Brand L, Eggeling C, Zander C, Drexhage KH, Seidel CAM. Journal of Physical Chemistry 1997;101:4313.
[7] Eggeling C, Widengren J, Rigler R, Seidel CAM. In: Rettig W, Strehmel B, Schrader S, Seifert H, editors. Applied fluorescence in chemistry, biology and medicine. Berlin: Springer; 1999 [Chapter 10].
[8] Li J, Chen P. Chinese Chemical Letters 1996;7(12):1121.
[9] Chibisov AK, Zakharova GV. Journal of the Chemical Society Faraday Transaction 1996;92:4917.
[10] Kopaindky B, Qiu P. Applied Physics 1982;B29:15.
[11] Li J, Chen P, Zhao J. Photographic Sci and Photochem (Chinese) 1996;14(4):314.
[12] Zaitsev A, Yang X. Journal of the American Chemical Society 1992;114:793.
[13] Tatikolov AS, Dzhulibekov KS. Journal of Physical Chemistry 1995;99:6525.
[14] Zuo Y, Yao S. Journal of Photochemistry and Photobiology B: Biology 1992;16(2):215.
[15] Stewart JJP. Journal of Computing Chemistry 1989; 10:209.
[16] Dewar MJS, Zoebisch EG, Healy EF, Stewart JJP. Journal of the American Chemical Society 1985;107:3902.
[17] West W, Gilman PB. In: James TH, editor. The theory of the photographic process. 4th ed. New York: Macmillan Publishing, Inc.; 1977 [Chapter 10].
[18] Serpone N, Sahyun MRV. Journal of Physical Chemistry 1994;98:734.
[19] Noukakis D, Auweraer M, Toppet S, De Schryver FC. Journal of Physical Chemistry 1995;99:11860.